Proceedings of the ASME 2014 Power Conference
POWER2014
July 28-31, 2014, Baltimore, Maryland, USA

POWER2014-32053

NUMERICAL SIMULATION OF STALL DEVELOPMENT INTO SURGE AND STALL CONTROL USING AIR INJECTION IN CENTRIFUGAL COMPRESSORS

Taher Halawa
Mechanical Engineering Department, UBC-University of British Columbia, Vancouver, B.C., Canada

Mohamed Alqaradawi
Mechanical & Industrial Engineering Department, Qatar University, Doha, Qatar

Osama Badr
Mechanical Engineering Department, British University, Cairo, Egypt

Mohamed S. Gadala
Mechanical Engineering Department, UBC-University of British Columbia, Vancouver, B.C., Canada

ABSTRACT

This study presents a numerical simulation of the formation of rotating stall and the initiation of surge in order to study the connection between stall and surge in centrifugal compressors. Also, the current paper introduces an optimization of the air injection method as a way to increase the surge margin. Results showed that during stall, the compressor is exposed to velocity and pressure fluctuations varying with time, and these fluctuations are increased suddenly and causing surge initiation. The major part which is responsible for the sudden increase in fluctuations is the vaneless region because it was found that the problem starts at the impeller exit near the shroud surface and then transfers to the impeller inlet. Results also showed that during surge, forces on the impeller blades increase to nearly double of its initial value and then decrease again. By using air injection at the vaneless region with different injection angles, it was found that injection with angle of 30° has a good effect on preventing surge and minimizing the pressure fluctuations comparing to other injection angles results. Results showed finally that the surge margin can be increased by using the injection with angle of 30° and with injection mass flow rate of 1% of the design inlet mass flow rate and this causes the surge limit to shift from 4 kg/s to 3.9 kg/s.

1. INTRODUCTION

The efficiency of centrifugal compressors is depending on the operating condition which is related to the mass flow rate and rotational speed. The compressor safe working range is bounded between two limits which are the surge limit and choke limit corresponding to lower and higher mass flow rate than the designed value respectively. If the working condition is inside the safe region and near the surge limit, there is a possibility of formation of some flow disturbances known as stall cells which may develop with time and cause compressor surge with high pressure fluctuations.

Rotating stall is a phenomenon that happens when the flow separations occur at impeller blades, and these separation areas increase with time until it forms stall cells which can cause flow blockage and high pressure fluctuations on compressor blades [1, 2].

It is important to study and identify the events which appear during stall and the factors which cause performance deterioration and surge initiation. McDougall et al. [3] reported that there are two dimensional, long length scale disturbances which are called modes that appear when the compressor is working close to the surge limit, and these modes can develop slowly and rotate at speeds between 20% and 50% of the impeller speed. I. Day [4] presented an experimental study about the formation of spike disturbances during stall. It was shown that some flow disturbances with short length scale rotate with a speed nearly 70% of impeller speed. These disturbances, called spikes, can grow very quickly in a few rotor revolutions and form stall cells. The experimental results of [4] were recently confirmed by several experimental studies [5-8]. Vo et al. [9] investigated numerically rotating stall inception in an axial compressor, it was noted that the flow separation at impeller leading edge is the main cause of stall inception because this allows some flow to pass from the clearance at tip and this is called the tip leakage flow. This tip leakage flow is interacting with the main flow and causes blocking of the rotor blade passages.

At the early stage of stall formation, back flow starts to initiate from the diffuser and hits the impeller blades, and part of this flow comes from one of the impeller passages to enter the adjacent passage [10].

Increasing the surge margin or the compressor safe working range is required for delaying the stall inception and keeping the compressor stable at low mass flow rates, and this can be achieved by controlling the parameters which affect the growing of the stall cells. There are several methods to control stall and these methods are classified into two main categories which are the passive and active control methods. The passive control idea depends on changing or modifying the compressor geometry especially at the casing in order to minimize the tip leakage flow. On the other hand, the active control methodology depends on adding or attaching a device to control the flow behavior without making any modification to the main compressor geometry. The passive control method was found to increase the surge margin but in the same time cause large efficiency losses [11-14]. For the active control technique, the air injection method is providing the shift of surge limit to lower mass flow rates with relatively small losses in efficiency [15-17].

Feng et al. [18] investigated experimentally the effect of air injection on the performance improvement for a compressor cascade. The results showed that the air injection is affecting the end wall region in a positive way by decreasing the vortices and correcting the flow path with small losses in static pressure. Skoch [19] reported that using air injection at the vaneless region of a centrifugal compressor using injectors with adjusted injection angles or using control tubes results in increased surge margin. It was found that injecting air in the same direction of impeller rotation increases the surge margin by 12.7 % with injection mass flow rate of 0.9 % of the main flow mass flow rate, while injecting air in the reverse direction of impeller rotation needs relatively higher injection mass flow rates to achieve the same result but it is accompanied with relatively higher pressure losses. Skoch [20] studied the air injection of a centrifugal compressor at the hub surface between the impeller and diffuser using different angles of injection, and results proved that injecting the air towards the diffuser vane pressure sides gives better results that injection towards the suction sides. Lim et al. [21] made an experimental study on the effect of changing the injection profile for a low speed axial compressor. A comparison was made between injecting air continuously and making a discrete injection, and results showed that the controlled discrete injection can achieve additional extension of the surge margin and in the same time can reduce the total amount of the injected air comparing with the continuous injection. Hiller et al. [22] introduced an experimental analysis for the compressor behavior when using air injection with different injection mass flow rates and various injection temperatures. It was shown that increasing the injection mass flow rate more than 2% of the main flow rate has a significant effect on increasing the stability zone, and it was found also that the variation of the injected air temperature does not affect the compressor stability margin.

The main objectives of this paper are to (i) simulate the development of stall into surge in order to find the parameters which are causing this change and need to be controlled, and (ii) increase the compressor safe region by optimizing the efficiency of the air injection method in the way of varying the angle of injection at a specified injection mass flow rate.

2. SPECIFICATIONS OF THE CASE STUDY

The NASA CC3 transonic centrifugal compressor was chosen for performing the numerical simulations. Figure 1 shows picture of the impeller and diffuser of the NASA CC3 compressor.

Figure 1. NASA CC3 compressor [23]

McKain and Holbrook [24] provides complete information about the NASA CC3 compressor including the geometry and design parameters. Table 1 summarizes the main geometry dimensions and design conditions of this compressor. There is a lot of information available about flow behavior in the NASA CC3 compressor from previous studies [16, 19, 20, 25-28].

Table 1. Specifications of the NASA CC3 compressor

Geometry	Number of impeller main blades	15
	Number of impeller splitter blades	15
	Number of diffuser vanes	24
	Tip clearance	0.2 mm
	Impeller inlet tip diameter	210 mm
	Impeller exit tip diameter	431 mm
	Diffuser inlet diameter	465.5 mm
	Diffuser exit diameter	724 mm
Design conditions	Rotational speed	21,789 rpm
	Mass flow rate	4.54 kg/s
	Total pressure ratio	4:01
	Adiabatic Efficiency	83.30%

3. METHODOLOGY OF THE NUMERICAL COMPUTATION

The finite volume method was used to solve the governing equations of fluid flow using FLUENT [29]. The governing equations are the continuity equation, Navier Stokes equations, energy equation and the turbulence equations. For the turbulence modeling, the k- ε realizable model was used because it can give accurate results for the unsteady high speed flows with strong flow separations. The sliding mesh method was used to simulate the rotating zones and the static zones by modifying the mesh at each time step. Equation 1 describes the general governing equation for the sliding mesh model.

$$\frac{d}{dt}\int_V \rho\phi dV + \int_{\partial V} \rho\phi\left(\overline{u} - \overline{u}_g\right)\cdot d\overline{A} = \int_{\partial V} \Gamma\nabla\phi\cdot d\overline{A} + \int_V S_\phi dV \qquad (1)$$

Where ϕ is a symbol for any general flow variable and V is the mesh volume and ρ is the fluid density and $\overline{u}$ is the flow velocity vector and $\overline{u}_g$ is the mesh velocity of the moving mesh and Γ is the diffusion coefficient and S_ϕ is the source term of ϕ. The integration term over the volume at the left hand side in equation 1 can be calculated from equation 2 as follows:-

$$\frac{d}{dt}\int_V \rho\phi dV = \frac{(\rho\phi V)^{n+1} - (\rho\phi V)^n}{\Delta t} \qquad (2)$$

Where n , n+1 are representing the quantity at the current and next time step respectively, and the term V^{n+1} is calculated from equation 3

$$V^{n+1} = V^n + \frac{dV}{dt}\Delta t \qquad (3)$$

The idea is that the term *dV/dt* can be computed by the summation of dot product of the velocity and area for each face of the mesh cell volume as shown in equation 4.

$$\frac{dV}{dt} = \int_{\partial V} \overline{u}_g\cdot d\overline{A} = \sum_j^{n_f} \overline{u}_{g,j}\cdot\overline{A}_j \qquad (4)$$

Where n_f is the number of faces on the control volume and A_j is the j face area vector and $\overline{u}_g$ is the mesh velocity of the moving mesh.

Figure 2 shows the numerical model which is composed of three main parts; the inlet guide vane, the impeller, and the diffuser. Also, there is a bend at the exit of the diffuser where the flow exits from the bend in the axial direction or in other words is aligned with the axis of rotation.

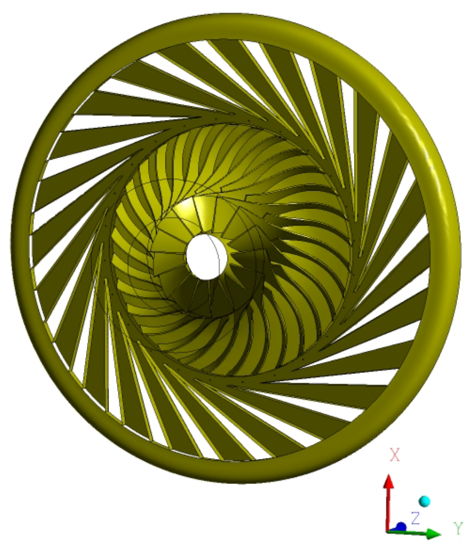

Figure 2. The compressor numerical model

3.1. Mesh Sensitivity Analysis

The aim of this analysis is to find the suitable mesh size that will give accurate results with the minimum error as possible. In order to simplify the problem, this test was done on a part of the whole geometry by using a part of the impeller and the corresponding part of the diffuser in order to save the computational time. Five mesh levels in the range between 550000 and 1505000 mesh elements were used for comparing with measurements [25]. Figure 3 indicates the variation of pressure with radial distance for all mesh cases and for the measurements. It can be noted that by increasing the number of mesh elements to be more than 1050000, the results remain the same and this means that this is the minimum level of the required accurate mesh. Based on that, the final number of mesh elements for the whole geometry that was used in the current study is 14 million cells in order to insure the results accuracy. The time step used in simulations is 2×10^{-6} second with 15 iterations per time step and it was increased in some cases to 20 iterations per time step; and the Courant number used was about 4 which achieved the solution stability and convergence.

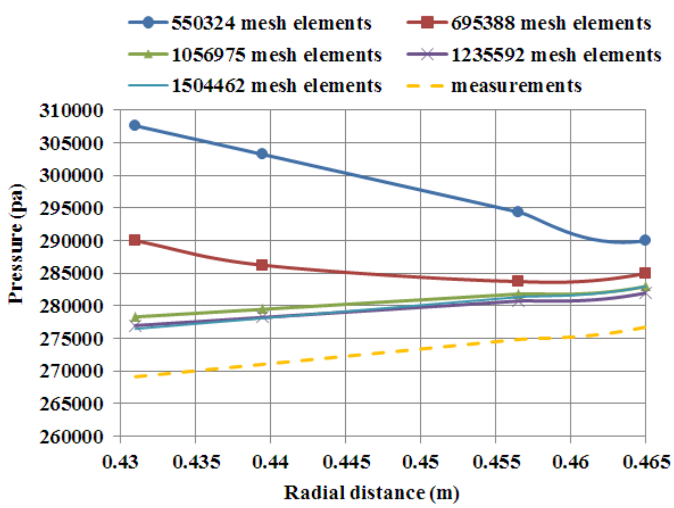

Figure 3. Pressure distribution for different mesh sets and for measurements

4. RESULTS

4.1. Validation of the CFD Numerical Model

The efficiency map of the compressor was generated by using the numerical model to solve at a specified flow rate; and the efficiency was calculated from the data obtained for pressure and temperature. Figure 4 shows the efficiency map for the numerical model results and also for measurements [25]. It can be noted that the numerical results are in good agreement with measurements, and there are small differences for the maximum efficiency values for the 70% and 80% speed curves. The numerical analysis shows a maximum efficiency of 85% while the corresponding measured value is 84%. This suggests that there is 1.2% relative error. Also, the maximum relative error between numerical results and measurements is 2% for points near the surge line.

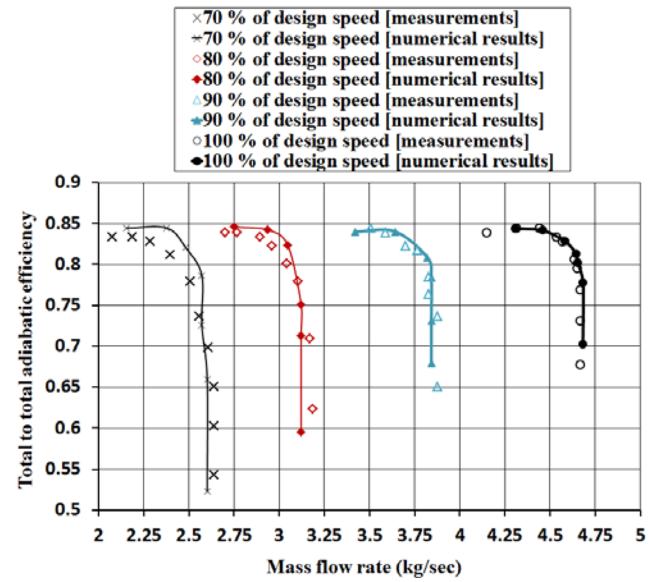

Figure 4. Compressor efficiency map (the numerical results versus measurements [25])

4.2. Stall and Surge Simulations

In order to simulate stall and surge, the numerical simulations were done at a point located inside the surge region corresponding to the design speed line at mass flow rate of 3.9 kg/s. When the stall starts, there are pressure and velocity fluctuations at some places in the compressor, especially near the shroud surface; and these fluctuations continue and may increase with time to cause surge. Figure 5 shows the fluid stream lines at 95% of the span length through the impeller and diffuser starting from stall inception condition up to condition after surge initiation. It can be noted from Fig.5 that the stream lines are normally distributed with little disturbances at diffuser exit and the vaneless region when stall initiates. After 5 rotor revolutions from the beginning of stall, flow separations start to appear at the impeller blades leading edge and the fluid deviates from the ideal flow path. After 7 rotor revolutions from stall initiation, separations are seen in most of the impeller passages; and the stream lines in the vaneless region become close to the tangential direction, and there is back flow in some of the diffuser passages. After 9 rotor revolutions, this is considered the beginning of surge because the number of diffuser passages with back flow increases, and there is a complete breakdown of flow distribution with complete back flow within 2 rotor revolutions from the beginning of surge.

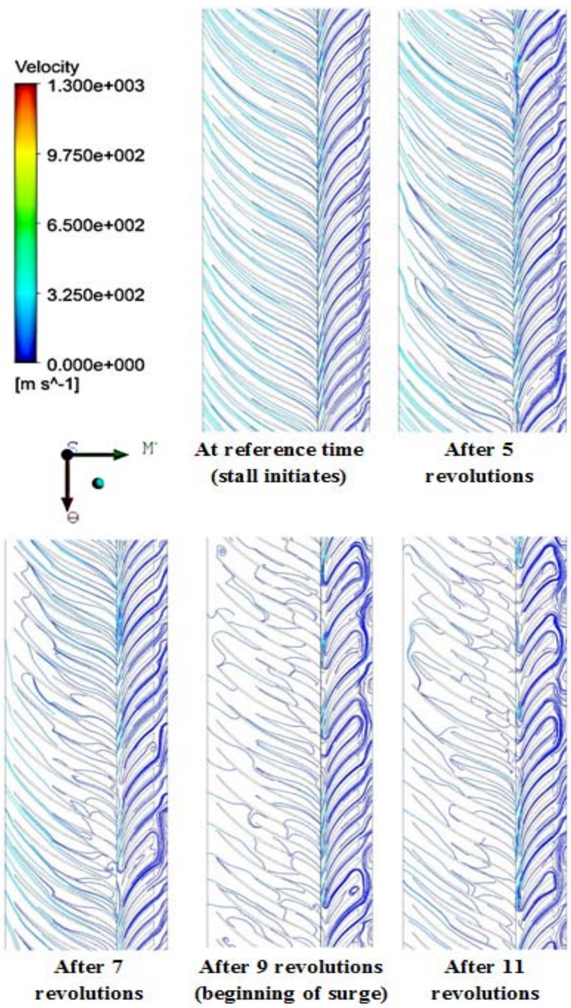

Figure 5. Stream lines distribution during stall and surge at location near shroud surface

It is important to monitor the flow at the tip clearance, because this gives an indication about the strength of the tip leakage flow. Five points located at the tip clearance gap above the impeller blades tip were selected in order to monitor the dynamic pressure as shown in Fig.6. Figure 7 shows the dynamic pressure variation with the number of time steps during stall at the five points selected and shown in Fig.6, where the time step used in simulations is $2x10^{-6}$ second. It can be noted from Fig.7 that for all pressure signals, there are fluctuations with time; and the amplitude of fluctuations varies from one point to another because there is a different pressure distribution for each point according to its location. The fluctuations at all points started at some time to increase suddenly and this is an indication of stall inception. Signals at points 1 and 2 have very large variations comparing with other points, and this means that the tip leakage flow at points 1 and 2 or at the impeller blades tip trailing edge is stronger comparing with other locations, and also this means that the problem of stall is coming from the vaneless region between the impeller exit and diffuser inlet.

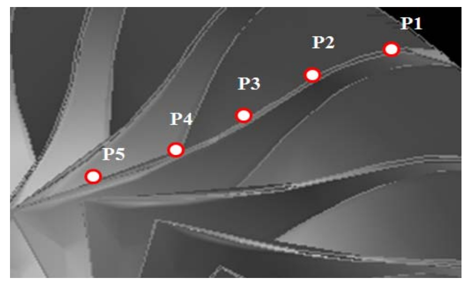

Figure 6. Location of the numerical monitor points at the tip clearance gap

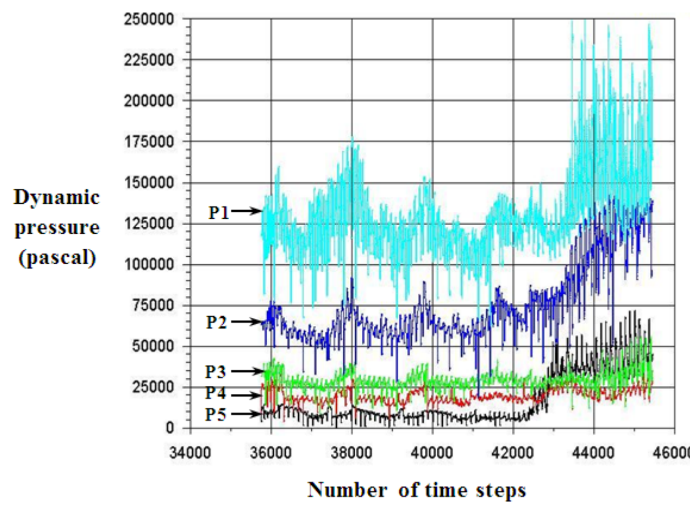

Figure 7. Dynamic pressure variation with time at points in the tip clearance gap

Based on the results shown in Fig.7, the vanless region may be the reason for the high pressure fluctuations at impeller exit, so, a point was selected in the vaneless region to monitor the pressure variation with time as shown in Fig.8.

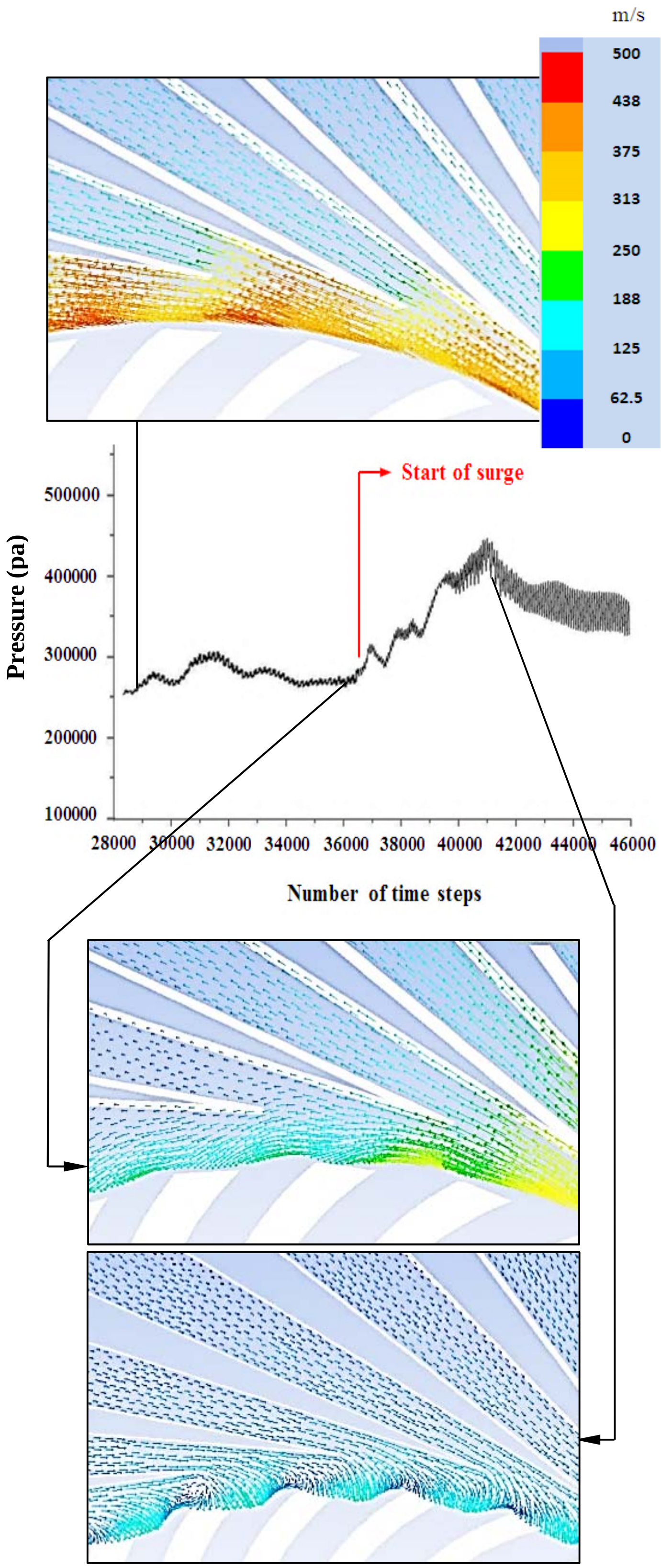

Figure 8. Pressure variation with time during stall and surge for a point in the vaneless region

It can be seen from Fig.8 that the pressure fluctuations develop with time from 250000 pa and reach 450000 pa and then decreases again to 350000 pa, and this is a part of the surge cycle when the back flow appears at the maximum pressure value in the curve, and this cycle is supposed to be repeated during surge. Figure 8 shows also velocity vectors for part of the vaneless region at three locations; before stall initiation, during stall and during surge. The velocity vectors before stall initiation are uniform without any deviation, but during stall, velocity vectors start to turn from some diffuser passages to the impeller. During surge, the velocity vectors show that the there is a complete back flow from the diffuser to the impeller.

Figure 9 indicates the pressure distribution at impeller blades surfaces at different time frames from stall to surge. The pressure distribution is slightly different for all blades, but after 5 rotor revolutions from stall initiation, there are some blades which are exposed to higher pressure than the other blades. After 7 rotor revolutions, regions of high pressure extend to the impeller blades leading edge, while after 9 revolutions corresponding to surge initiation, there are localized very high pressure regions at the blades tip near the trailing edge. This indicates that the problem of appearance of high pressure locations is coming from the vaneless region and then transfers to the impeller exit and then to impeller inlet.

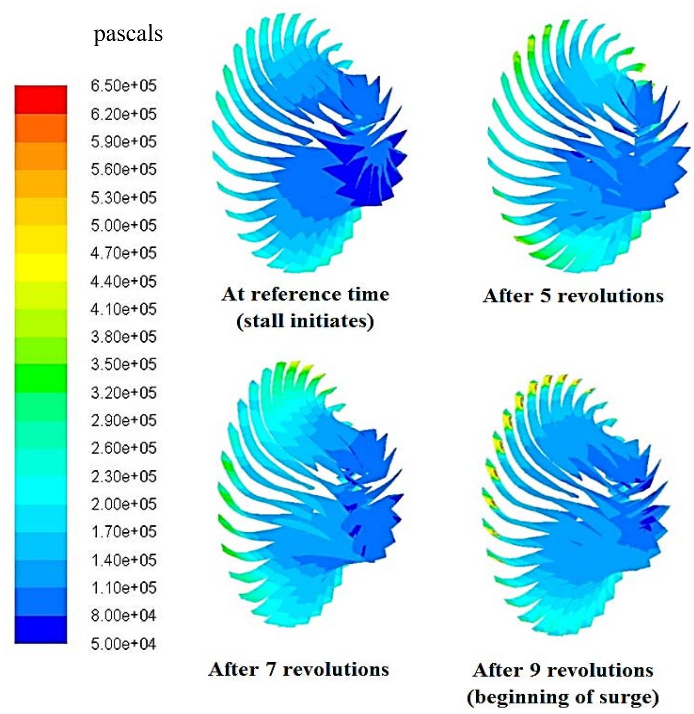

Figure 9. Pressure distribution on impeller blades and its variation with time

Pressure fluctuations during stall can be expressed in the form of forces. Figure 10 shows the variation of the force acting on the impeller blades in the axial direction with time during stall and surge.

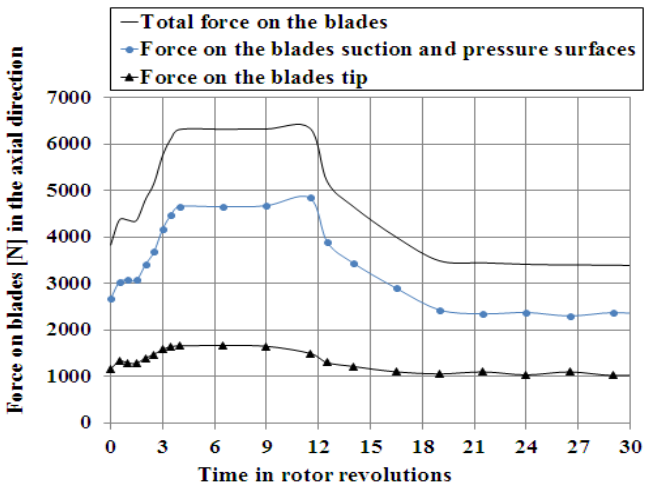

Figure 10. Variation of the force affecting impeller blades with time during surge

There are three curves indicating; the force on the tip of the blades, the force on suction and pressure blades surfaces, and finally the total force which equals the summation of the forces of the other two curves. It can be concluded from Fig.10 that the total force is increasing up to double of its initial value while the force acting on blades tip increases 1.5 times of its initial value during the surge event, and this increase in force is followed by another decrease as a part of the surge cycle which can be repeated with time, and this means that the blades may be damaged due to this strong variation in force.

4.3. Air Injection Simulations

The injection of air at the vaneless region was used in order to increase the surge margin of the compressor. Figure 11 shows the compressor configuration with indication of the air injection points at the shroud surface of the vaneless area between impeller and diffuser. Twelve points were selected because it is recommended to use at least 8 points of injection based on a previous study [19]. Figure 12 shows a clarification of the injection angle Θ at one of the injection points at the vaneless region. The air was selected to be injected with injection mass flow rates of 1% of the inlet design mass flow rate and with injection angles of 10°, 20°, 30°, 40°. The reason of using these specific injection angles is that it is required to find the best injection angle that will give the best results knowing that the previous studies done on this compressor were interested in two angles 0° of and 180° only [16, 19]. Also, the reason for selecting injection angle values as a multiple of 10° is that it is important to test the air injection performance when injecting air close to the diffuser vane angle which is 13.4°. So, air injection at angle of 10° and at angle of 20° represent the injection toward the pressure and suction sides of the diffuser vane respectively. In order to examine the effect of using more injection angles while keeping constant difference between any two injection angle values, the injection angles of 30° and 40° were also used.

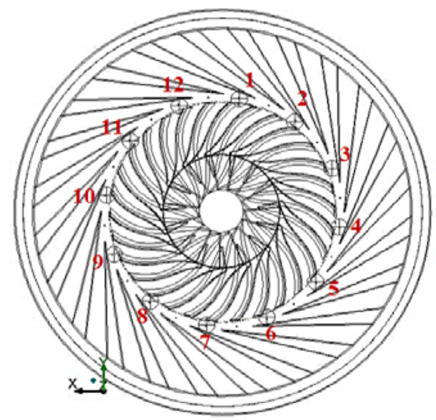

Figure 11. Air injection locations at the vaneless space

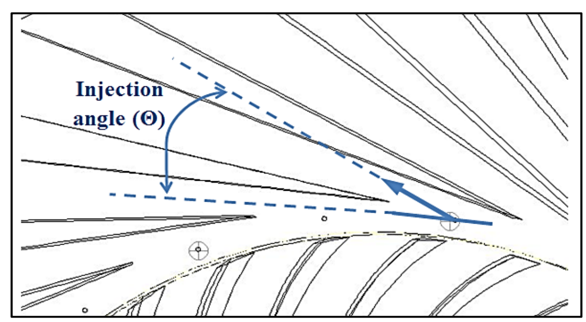

Figure 12. Representation of the angle of injection

The theoretical flow is a flow without any losses in the vaneless region where there is no losses in kinetic energy and no deviation in the fluid angle between the impeller exit (entrance of the vaneless region) and the diffuser inlet (the end of the vaneless region), but in reality, there are some losses in the vaneles region; and these losses become very large in the case of stall. Figures 13 and 14 show the variation of average fluid velocity and average fluid angle respectively with time at the diffuser inlet for all cases of injection and for the case of no injection. Figure 13 shows that there is a big drop in the kinetic energy for the case of injection angle of 10° and for the case of no injection. Also, these losses in the kinetic energy are increasing with time for the cases of injection of 20° and 40°. For the case of injection with angle of 30°, the kinetic energy losses are small relatively and seem to be nearly constant. Figure 14 indicates that there are very high fluctuations in the value of the fluid angle for the case of no injection, and there are relatively high fluctuations for all cases of injection except for the case of injection with angle of 30°, where the fluid angle is nearly constant and is always close to the diffuser vane angle value of 13.4°.

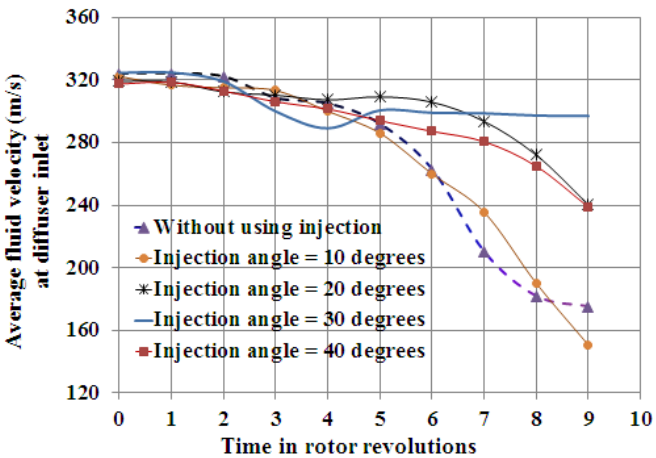

Figure 13. Velocity variation with time at diffuser inlet for different cases of injection

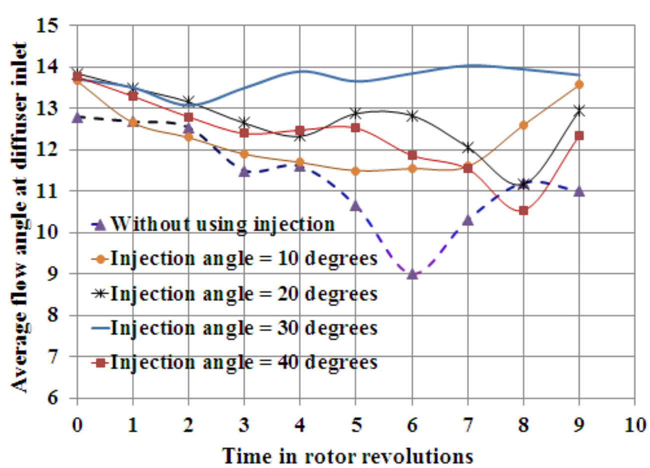

Figure 14. Flow angle variation with time at diffuser inlet for different cases of injection

Figures 15, 16, 17 and 18 show the fluid stream lines colored by velocity magnitude in m/s for the cases of injection angles of 10°, 20°, 30°, 40° respectively at time corresponding to 20 rotor revolutions after the initiation of the rotating instabilities.

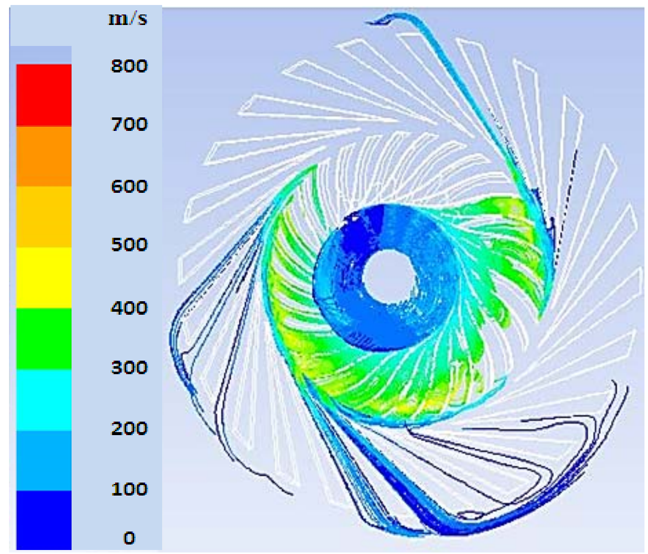

Figure 15. Stream lines distribution after 20 revolutions from stall initiation for the case of injection with angle of 10°

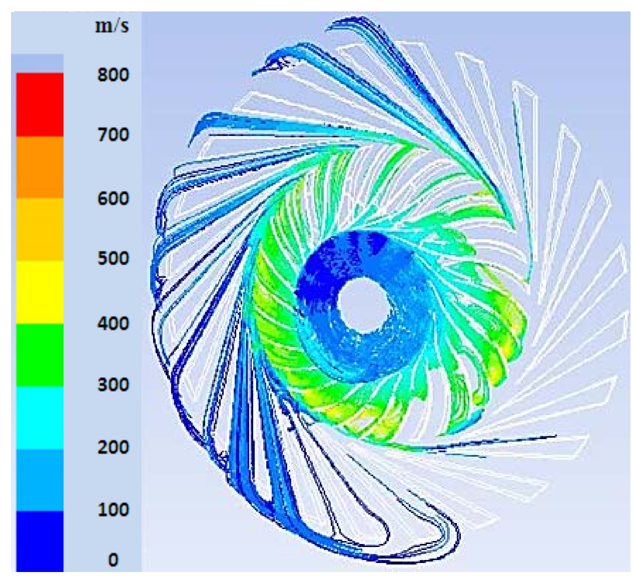

Figure 16. Stream lines distribution after 20 revolutions from stall initiation for the case of injection with angle of 20°

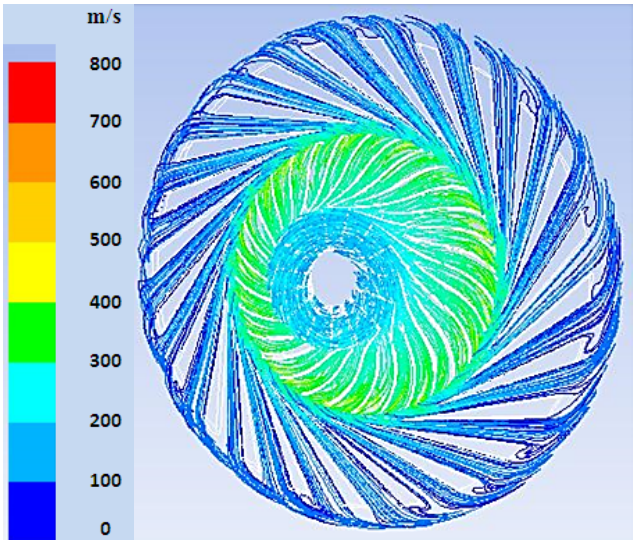

Figure 17. Stream lines distribution after 20 revolutions from stall initiation for the case of injection with angle of 30°

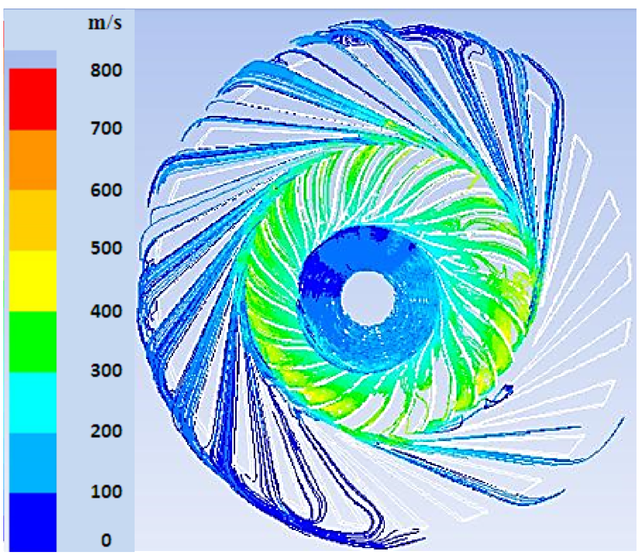

Figure 18. Stream lines distribution after 20 revolutions from stall initiation for the case of injection with angle of 40°

It can be noted that all the cases with injection are subjected to surge except the case of injection with angle of 30°, because when looking at figures 15, 16 and 18, there is complete recirculation of the stream lines inside the impeller passages and the fluid fails to enter most of the diffuser passages. On the other hand, for the case of injection with angle of 30° (Fig.17), the stream lines distribution is uniform and the solution is nearly steady with small separations at the exit of the diffuser.

Figure 19 shows the forces acting on impeller blades for different cases of injection and for the case of no injection; it is shown that the case of injection with angle of 30° achieves the compressor stabilization because the force is fluctuating around a fixed value without the sudden rise which appears in the other cases.

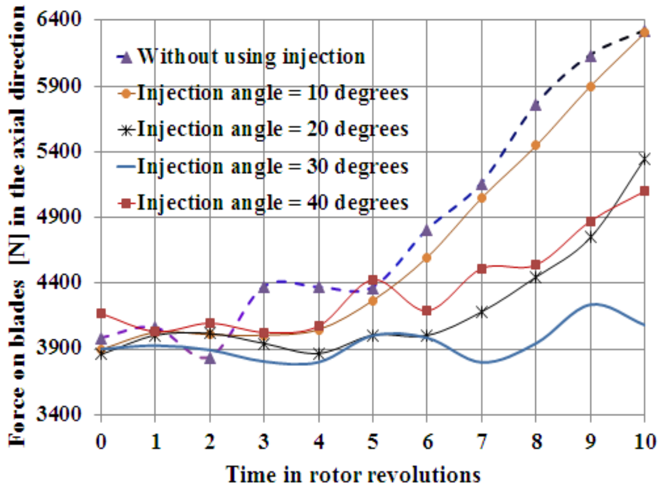

Figure 19. Force variation with time for different cases of injection

5. CONCLUSIONS

(1) During stall, fluid stream lines variation showed that the formation of stall is starting from the impeller inlet where flow separations take place; and in some impeller passages, there is a strong fluid deviation from the blades surface, while in other impeller passages, the fluid distribution is normal, and this causes the fluid to exit from impeller with angle and velocity magnitude differ from one passage to another. This non uniformity in the flow behavior at impeller exit causes formation of high pressure regions and random flow in the vaneless region, and this is considered the moment of stall development.

(2) There is a possible connection between stall and surge because the stall is causing flow deterioration at the vaneless region, and this causes back flow formation in some diffuser passages and strong pressure fluctuations to appear at the vaneless region and then move to the impeller blades. For that reason, the vaneless region may be the main reason of surge initiation.

(3) Air injection method is an effective method for increasing the safe region of the compressor and when using air injection angle larger than the diffuser vane angle, forces acting on the impeller blades are reduced comparing with injecting air at angles lower than the diffuser vane angle.

(4) By injecting air at an angle of 30° and with injection mass flow rate of 1% of the design inlet mass flow rate, the forces on blades are maintained constant and the flow is stabilized at an operating condition inside the surge margin corresponding to a mass flow rate of 3.9 kg/s.

(5) As a suggestion for future studies, it is important to make an optimization of the air injection parameters by using several values of the injection mass flow rate, and also by varying the injection angle with interval difference value less than 10°.

ACKNOWLEDGMENTS

This research was supported by a NPRP grant No. 4-651-2-242 from the Qatar National Research Fund (a member of Qatar Foundation), Doha, Qatar.

REFERENCES

[1] E. M. Greitzer, "Surge and rotating stall in axial flow compressors—Part I: Theoretical compression system model," *Journal of Engineering for Power,* vol. 98, p. 190, 1976.

[2] J. M. Haynes, G. J. Hendricks, and A. H. Epstein, "Active stabilization of rotating stall in a three-stage axial compressor," *ASME Transactions Journal of Turbomachinery,* vol. 116, pp. 226-239, 1994.

[3] N. M. McDougall, N. Cumpsty, and T. Hynes, "Stall inception in axial compressors," *Journal of Turbomachinery,* vol. 112, pp. 116-125, 1990.

[4] I. Day, "Stall inception in axial flow compressors," *Journal of Turbomachinery,* vol. 115, pp. 1-9, 1993.

[5] A. Deppe, H. Saathoff, and U. Stark, "Spike-type stall inception in Axial Flow Compressors," in *6th Conference on Turbomachinery, Fluid Dynamics and Thermodynamics, Lille, France*, 2005.

[6] C. Hah, J. Bergner, and H.-P. Schiffer, "Short length-scale rotating stall inception in a transonic axial compressor-criteria and mechanisms," *ASME Paper GT2006-90045,* 2006.

[7] H. Saxer-Felici, A. Saxer, A. Inderbitzin, and G. Gyarmathy, "Prediction and measurement of rotating stall cells in an axial compressor," *Journal of Turbomachinery,* vol. 121, pp. 365-375, 1999.

[8] S. Weichert and I. Day, "Detailed measurements of spike formation in an axial compressor," *Journal of Turbomachinery,* vol. 136, p. 051006, 2014.

[9] H. D. Vo, C. S. Tan, and E. M. Greitzer, "Criteria for spike initiated rotating stall," *Journal of Turbomachinery,* vol. 130, 2008.

[10] G. Gu, A. Sparks, and S. S. Banda, "An overview of rotating stall and surge control for axial flow compressors," *Control Systems Technology, IEEE Transactions on,* vol. 7, pp. 639-647, 1999.

[11] M. Hembera, H.-P. Kau, and E. Johann, "Simulation of casing treatments of a transonic compressor stage," *International Journal of Rotating Machinery,* vol. 2008, 2008.

[12] T. H. IVOR DAY, "Stability Enhancement by Casing Grooves: The Importance of Stall Inception Mechanism and Solidity," *Journal of Turbomachinery,* vol. 134, 2012.

[13] X. Lu, W. Chu, J. Zhu, and Y. Zhang, "Numerical Investigations of the Coupled Flow through a Subsonic Compressor Rotor and Axial Skewed Slot," *Journal of Turbomachinery,* vol. 131, 2009.

[14] C.-Y. Park, Y.-S. Choi, K.-Y. Lee, and J.-Y. Yoon, "Numerical study on the range enhancement of a centrifugal compressor with a ring groove system," *Journal of mechanical science and technology,* vol. 26, pp. 1371-1378, 2012.

[15] B. Beheshti, B. Farhanieh, K. Ghorbanian, J. Teixeira, and P. Ivey, "Performance enhancement in transonic axial compressors using blade tip injection coupled with casing treatment," *Proceedings of the Institution of Mechanical Engineers, Part A: Journal of Power and Energy,* vol. 219, pp. 321-331, 2005.

[16] J.-P. Chen, R. S. Webster, M. D. Hathaway, G. P. Herrick, and G. J. Skoch, "High performance computing of compressor rotating stall and stall control," *Integrated Computer-Aided Engineering,* vol. 16, pp. 75-89, 2009.

[17] H. Khaleghi, M. Boroomand, J. Teixeira, and A. Tousi, "A numerical study of the effects of injection velocity on stability improvement in high-speed compressors," *Proceedings of the Institution of Mechanical Engineers, Part A: Journal of Power and Energy,* vol. 222, pp. 189-198, 2008.

[18] D. Feng, F. Chen, Y. Song, H. Chen, and Z. Wang, "Enhancing aerodynamic performances of highly loaded compressor cascades via air injection," *Chinese Journal of Aeronautics,* vol. 22, pp. 121-128, 2009.

[19] G. J. Skoch, "Experimental investigation of centrifugal compressor stabilization techniques," *Transactions of the ASME-T-Journal of Turbomachinery,* vol. 125, pp. 704-713, 2003.

[20] G. J. Skoch, "Experimental investigation of diffuser hub injection to improve centrifugal compressor stability," DTIC Document2004.
[21] H.-S. Lim, H.-J. Bae, Y.-C. Lim, S.-J. Song, S.-H. Kang, and S.-S. Yang, "Injection profile effects on low speed axial compressor stability enhancement," *Journal of mechanical science and technology,* vol. 25, pp. 1501-1507, 2011.
[22] S.-J. Hiller, R. Matzgeller, and W. Horn, "Stability enhancement of a multistage compressor by air injection," *Journal of Turbomachinery,* vol. 133, 2011.
[23] G. J. Skoch, "Centrifugal Compressor Flow Range Extension Using Diffuser Flow Control," *NASA Glenn Research Center, Cleveland, Ohio, Dec,* vol. 5, p. 17, 2000.
[24] T. F. McKain and G. J. Holbrook, *Coordinates for a high performance 4: 1 pressure ratio centrifugal compressor*: National Aeronautics and Space Administration, 1997.
[25] G. J. Skoch, P. Prahst, M. Wernet, J. Wood, and A. Strazisar, "Laser Anemometer Measurements of the Flow Field in a 4: 1 Pressure Ratio Centrifugal Impeller," DTIC Document1997.
[26] Z. Spakovszky, "Backward Traveling Rotating Stall Waves in Centrifugal Compressors (2002-GT-30379)," *Journal of Turbomachinery,* pp. 1-12, 2004.
[27] D. L. Tarr, "Scaling of impeller response to impeller-diffuser interactions in centrifugal compressors," Massachusetts Institute of Technology, 2008.
[28] M. P. Wernet, M. M. Bright, and G. J. Skoch, "An investigation of surge in a high-speed centrifugal compressor using digital PIV," *TRANSACTIONS-AMERICAN SOCIETY OF MECHANICAL ENGINEERS JOURNAL OF TURBOMACHINERY,* vol. 123, pp. 418-428, 2001.
[29] A. FLUENT, "13.0. ANSYS," *Inc., Canonsburg, PA, USA,* 2011.